Hindawi Publishing Corporation
Journal of Nanomaterials
Volume 2014, Article ID 979875, 7 pages
http://dx.doi.org/10.1155/2014/979875

Research Article

Fractional Contributions of Defect-Originated Photoluminescence from $CuInS_2$/ZnS Coreshells for Hybrid White LEDs

Quinton Rice,[1] Sangram Raut,[2,3] Rahul Chib,[2] Zygmunt Gryczynski,[2,3] Ignacy Gryczynski,[2] Wenjin Zhang,[4] Xinhua Zhong,[4] Mahmoud Abdel-Fattah,[1] Bagher Tabibi,[1] and Jaetae Seo[1]

[1] *Department of Physics, Advanced Center for Laser Science and Spectroscopy, Hampton University, Hampton, VA 23668, USA*
[2] *Department of Cell Biology and Immunology, Center for Fluorescence Technologies and Nanomedicine, University of North Texas Health Science Center, Fort Worth, TX 76107, USA*
[3] *Department of Physics and Astronomy, Texas Christian University, Fort Worth, TX 76129, USA*
[4] *Department of Chemistry, Key Laboratory for Advanced Materials, East China University of Science and Technology, Shanghai 200237, China*

Correspondence should be addressed to Jaetae Seo; jaetae.seo@hamptonu.edu

Received 27 July 2014; Revised 10 September 2014; Accepted 10 September 2014; Published 22 October 2014

Academic Editor: Ruibing Wang

Copyright © 2014 Quinton Rice et al. This is an open access article distributed under the Creative Commons Attribution License, which permits unrestricted use, distribution, and reproduction in any medium, provided the original work is properly cited.

The wide optical tunability and broad spectral distribution of $CuInS_2$/ZnS (CIS/ZnS) coreshells are key elements for developing the hybrid white light emitting diodes where the nanoparticles are stacked on the blue LEDs. Two $CIS/ZnS_{555\,nm}$ and $CIS/ZnS_{665\,nm}$ coreshells are utilized for the hybrid white LED development. The time-resolved spectroscopy of $CIS/ZnS_{555\,nm}$ and $CIS/ZnS_{665\,nm}$ reveals the correlation between the fast, intermediate, and slow decay components and the interface-trapped state and shallow- and deep-trapped states, although the fractional amplitudes of photoluminescence (PL) decay components are widely distributed throughout the entire spectra. The temperature-resolved spectroscopy explains that the PL from deep-trapped donor-acceptor (DA) state has relatively large thermal quenching, due to the relative Coulomb interaction of DA pairs, compared to the thermal quenching of PL from interface defect state and shallow-trapped DA state. A good spectral coupling between the blue diode excitation and the PL from CIS/ZnS leads to the realization of hybrid white LEDs.

1. Introduction

Light emitting devices (LEDs) are a key element in the photonic and optoelectronic devices including optical displays, room lighting, cell phones, motor vehicle head lights and indicators, and traffic lights. The spectral distribution and purity of optical materials lead to the realization of photonic and optoelectronic applications. The broad spectral distribution is required for white LEDs, and the spectral purity is required for photonic color indicator or displays. Semiconductor nanocrystals (SNCs) are of significant interest in developing LEDs [1–3] because of their wide optical tunability and good photostability. The quantum confinement in the SNCs with sizes near the bulk Bohr radius provides wide optical tunability with strong blue-shift of optical bandgap [4]. The SNCs have good photostability with less photobleaching compared to organic materials. The II–VI SNCs have a wide optical tunability, good photostability, and high color purity, but heavy metals and narrow spectral width are undesirable for white LED development [5]. The I–III-VI_2 SNCs have a broad emission spectral width, wide optical tunability, and good photostability in addition to no toxicity associated with the heavy metals including cadmium or lead chalcogenides. Therefore, the I–III-VI_2 SNCs are excellent optical materials for hybrid white LED development.

The emission of II–VI SNCs mainly comes from the exciton pair recombination in the conduction and valence bands and possibly the transitions from/to surface-trapped state just below the conduction band or above the valence band [6]. The emission of I–III-VI_2 SNCs comes from

the optical transitions related surface-trapped state for core materials, interface-trapped state for coreshells, and shallow- and deep-trapped donor-acceptor (DA) states [7]. The interface-trapped state and shallow- and deep-trapped DA states are correlated to the emissions at the higher, intermediate, and lower energy spectral region, respectively [8, 9]. However, the numerous interface and interstitial and vacancy on/in the large numbers of coreshells lead to the broad optical spectrum and even overlap all emissions from the interface-trapped state and defect-related DA-trapped state [10–12].

In this paper, two selective I–III-VI_2 coreshells of $CuInS_2/ZnS_{665\,nm}$ ($CIS/ZnS_{665\,nm}$) and $CuInS_2/ZnS_{555\,nm}$ ($CIS/ZnS_{555\,nm}$) with photoluminescence (PL) peaks ~555 nm and ~665 nm, respectively, are utilized for the hybrid white LED development. The temperature-dependent and time-resolved PL studies on the $CIS/ZnS_{665\,nm}$ coreshells reveal the contributions of interface-trapped state and defect-related DA-trapped state to the PL spectra, while the optical studies on the $CIS/ZnS_{555\,nm}$ coreshells illustrate the modification of PL decays and spectral symmetry. Finally, the time-resolved and temperature-dependent PL studies of $CIS/ZnS_{665\,nm}$ and $CIS/ZnS_{555\,nm}$ describe the optical origins of better spectral covering and spectral coupling for developing hybrid white LEDs, where the SNCs are stacked on the blue LEDs for the excitation as well as the spectral coupling in the entire visible spectral region.

2. Experimental Details

The $CIS/ZnS_{665\,nm}$ and $CIS/ZnS_{555\,nm}$ coreshells were prepared by the literature procedure [13]. The absorption spectrum of CIS/ZnS SNCs was measured with a UV-VIS spectrophotometer (Cary 50 Bio, Varian Inc.) and a UV-VIS spectrometer (Agilent 8453). The photoluminescence excitation (PLE) spectra were collected using spectrofluorometer (Cary Eclipse, Varian Inc.) while the PL was monitored at 525 nm, 550 nm, and 600 nm using appropriate narrow band-pass filters for $CIS/ZnS_{555\,nm}$ and at 650 nm, 575 nm, 640 nm, and 690 nm for $CIS/ZnS_{665\,nm}$.

The PL lifetimes of CIS/ZnS were recorded using a FluoTime 200 fluorometer (PicoQuant, Inc.) with a diode laser excitation at ~470 nm, which has a pulse width less than ~70 ps and 100 KHz repetition rate. A long-wavelength pass (LWP) filter at 495 nm was used to exclude the laser excitation light. The selective PL wavelengths for measuring lifetimes were 525 nm, 550 nm, and 650 nm for $CIS/ZnS_{555\,nm}$ and CIS/ZnS and 575 nm, 640 nm, and 690 nm for $CIS/ZnS_{665\,nm}$ to study the fractional contribution of interface-trapped state and defect-related shallow- and deep-trapped DA states to the PL. The tail fitting with multiexponential decay equation and nonlinear least square function to the PL decay measurements was used to extract the PL lifetimes as Seo et al. described [14]. The multiexponential decay equation of emission intensity $I(\lambda, t)$ at the time (t) and wavelength (λ) is [14]

$$I(\lambda, t) = I_0(\lambda, t = 0) \sum a_i e^{-t/\tau_i}, \quad (1)$$

where τ_i is the characteristic lifetime of the ith decay component, a_i is the subsequent decay amplitude, and $I_0(\lambda)$ is the fluorescence intensity at time $t = 0$. The intensity weighted average lifetime is given by [14]

$$\langle \tau \rangle_{\text{int}} = \frac{\sum a_i \tau_i^2}{\sum a_i \tau_i} = \sum_i f_i \tau_i, \quad (2)$$

where $f_i = a_i \tau_i / \sum a_i \tau_i$ is the fractional contribution of each decay component to $I_0(\lambda)$ and the denominator $\sum a_i \tau_i$ is over all amplitudes and decay times which is proportional to the total intensity.

The temperature-dependent PL of CIS/ZnS was detected using optical fibers (Ocean Optics, P600-VIS-NIR) and a spectrometer (Ocean Optics, USB4000) with a spectral resolution of ~1 nm. A HeCd laser at 325 nm was used as an excitation source. The laser power was ~9 mW with a beam chopper operating at a frequency of 300 Hz. The SNC materials were placed between two quartz microglasses on the cold finger in the helium closed-cycle cryostat (Janis, SHI-4-1).

3. Result

Figure 1 shows absorption, PL, and PLE spectra of CIS/ZnS coreshells. The absorption spectra of coreshells have a strong blue-shift from the optical bandgap (~1.5 eV/~827 nm) of bulk CIS due to quantum confinement [15]. The PLE spectra of $CIS/ZnS_{555\,nm}$ displayed broad shoulders at ~470 nm and ~480 nm for the monitoring PL wavelengths at ~525 nm, ~550 nm, and ~600 nm. It indicates the broad spectral contribution from the interface-trapped state and defect-related DA-trapped state to the PL of CIS/ZnS. However, the broad PLE shoulder disappeared or was reduced for $CIS/ZnS_{665\,nm}$ which implies that the wide size distribution and various types of defect play a role in the further spectral broadening of PLE [16]. The absorption and PLE spectra of CIS/ZnS did not exhibit the multiple distinct peaks which could be observed from the II–VI SNCs with sizes near the bulk Bohr radius as a result of quantum confinement [17]. The optical transitions in II–VI SNCs are mainly related to the exciton pair recombination in the conduction and valence bands [18], and surface-trapped state, while those of I–III-VI_2 are related to the surface/interface-trapped state and defect-related DAP recombination [15, 19, 20]. The PL spectra of $CIS/ZnS_{555\,nm}$ and $CIS/ZnS_{665\,nm}$ exhibit the peaks at ~555 nm and ~665 nm, which are attributed to the interface-trapped state and shallow- and deep-trapped DA states. The full width at half maximum (FWHM) of PL spectrum from $CIS/ZnS_{665\,nm}$ at 300 K is ~115 nm and that of $CIS/ZnS_{555\,nm}$ at 300 K is ~100 nm. The PL from $CIS/ZnS_{555\,nm}$ has a better spectral coupling with the blue excitation for generating white light in the visible spectral region while $CIS/ZnS_{665\,nm}$ has the undesired infrared emission which is similar to the previous reports [21]. The asymmetry of PL spectrum and the reduced spectral width of the $CIS/ZnS_{555\,nm}$ compared to the PL properties of $CIS/ZnS_{665\,nm}$ are due to the higher contributions from the interface-trapped state and shallow-trapped DA state in the lower wavelength spectral region and

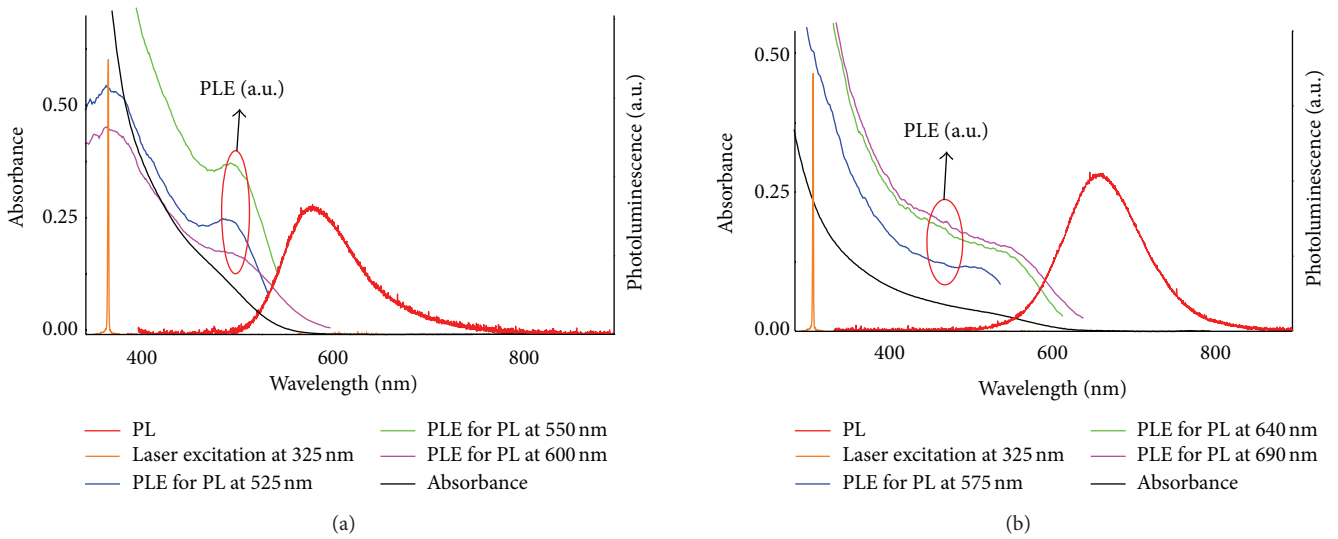

FIGURE 1: Absorption, PLE, and PL spectra of (a) CIS/$ZnS_{555\,nm}$ and (b) CIS/$ZnS_{665\,nm}$.

the less size-dependent confinement of deep-trapped state. Therefore, the time-resolved and temperature-dependent PL studies of CIS/$ZnS_{665\,nm}$ and CIS/$ZnS_{555\,nm}$ are required to explain the optical origins of spectral covering and coupling for developing hybrid white LEDs.

Figure 2 shows the PL decays (top), residual traces (middle), and decay components (bottom) from CIS/$ZnS_{665\,nm}$ at shorter wavelength, 575 nm (a), center wavelength, 640 nm (b), and longer wavelength, 690 nm (c). The PL at 575 nm has three exponential decay times with fast (τ_1), intermediate (τ_2), and slow (τ_3) components of ~13.8 ns, ~51.2 ns, and ~180.1 ns with the fractional amplitudes of 69.8%, 27.1%, 3.1%, respectively. The PL decays at 640 nm have fast (τ_1), intermediate (τ_2), and slow (τ_3) components of ~15.4 ns, ~71.1 ns, and ~236.8 ns with the fractional amplitudes of 55.4%, 38.1%, and 6.5%, respectively. The PL decays at 690 nm have fast (τ_1), intermediate (τ_2), and slow (τ_3) components of ~37.6 ns, ~137.9 ns, and ~367.3 ns with the fractional amplitudes of 41.0%, 49.3%, and 9.7%, respectively. The averaged lifetimes of three exponential decays of CIS/$ZnS_{665\,nm}$ are ~29.1 ns, ~51.0 ns, and ~119.0 ns at the PL wavelengths 575 nm, 640 nm, and 690 nm, respectively. The fast lifetime (τ_1) with larger fractional amplitude at the shorter wavelength as shown in Figure 2(a) is related to the interface defect state [15, 19, 20]. The fractional amplitude of slow decay (τ_3) increases at longer wavelength as shown in the Figure 2(c) component. This suggests that the slow decay is related to the deep-trapped DA state [22]. Then, the intermediate (τ_2) decay component in the broad spectral region as shown in Figures 2(a), 2(b), and 2(c) is possibly assigned to the shallow-trapped DA state which is strongly overlapped with interface-tapped state and deep-trapped state. The fractional amplitude of fast (τ_1) decay component is decreased at longer wavelength and that of intermediate (τ_2) and slow (τ_3) components is increased at longer wavelength. The fast (τ_1) and intermediate (τ_2) decay components have large fractional amplitudes in the entire spectral region. It implies that interface-trapped state and shallow-trapped DA state provide the major contribution to the PL.

Figure 3 shows the PL decays (top), residual traces (middle), and decay components (bottom) from CIS/$ZnS_{555\,nm}$ at shorter wavelength, 525 nm (a), center wavelength, 550 nm (b), and longer wavelength, 600 nm (c), to analyze the contributions of interface defect-related state and shallow- and deep-trapped defect-related DA states. The PL at 525 nm has three exponential decay times with fast (τ_1), intermediate (τ_2), and slow (τ_3) components of ~17.3 ns, ~116.3 ns, and ~428.9 ns with the fractional amplitudes of 48.8%, 40.3%, and 10.9%, respectively. The PL decays at 550 nm have fast (τ_1), intermediate (τ_2), and slow (τ_3) components of ~23.5 ns, ~160.8 ns, and ~565.8 ns with the fractional amplitudes of 49.8%, 43.4%, and 7.9%, respectively. The PL decays at 600 nm have fast (τ_1), intermediate (τ_2), and slow (τ_3) components of ~20.2 ns, ~184.0 ns, and ~575.4 ns with the fractional amplitudes of 42.2%, 45.6%, and 12.2%, respectively. The fractional amplitudes of fast (τ_1) PL decay are slightly decreased, but those of intermediate (τ_2) PL decay are slightly increased. However, both fractional amplitudes of fast (τ_1) and intermediate (τ_2) decays have the major contributions to the PL and are widely distributed in the entire spectral region. It indicates that the interface-trapped state and shallow-trapped DA state are strongly overlapped. The average lifetimes of three exponential decays of CIS/$ZnS_{555\,nm}$ are ~101.9 ns, ~124.3 ns, and ~162.3 ns at the PL wavelengths 525 nm, 550 nm, and 600 nm, respectively. The averaged PL lifetimes of CIS/$ZnS_{555\,nm}$ are longer than those of CIS/$ZnS_{665\,nm}$. It implies that CIS/$ZnS_{555\,nm}$ has less PL quenching through a nonradiative decay process.

The thermal quenching properties of PL from CIS/$ZnS_{555\,nm}$ and CIS/$ZnS_{665\,nm}$ make further confirmation on the implication of defect-related interface-trapped state and shallow- and deep-trapped DA states to PL distribution. The temperature-dependent PLs from CIS/$ZnS_{665\,nm}$ (a) and CIS/$ZnS_{555\,nm}$ (b) are shown in Figure 4. The insets

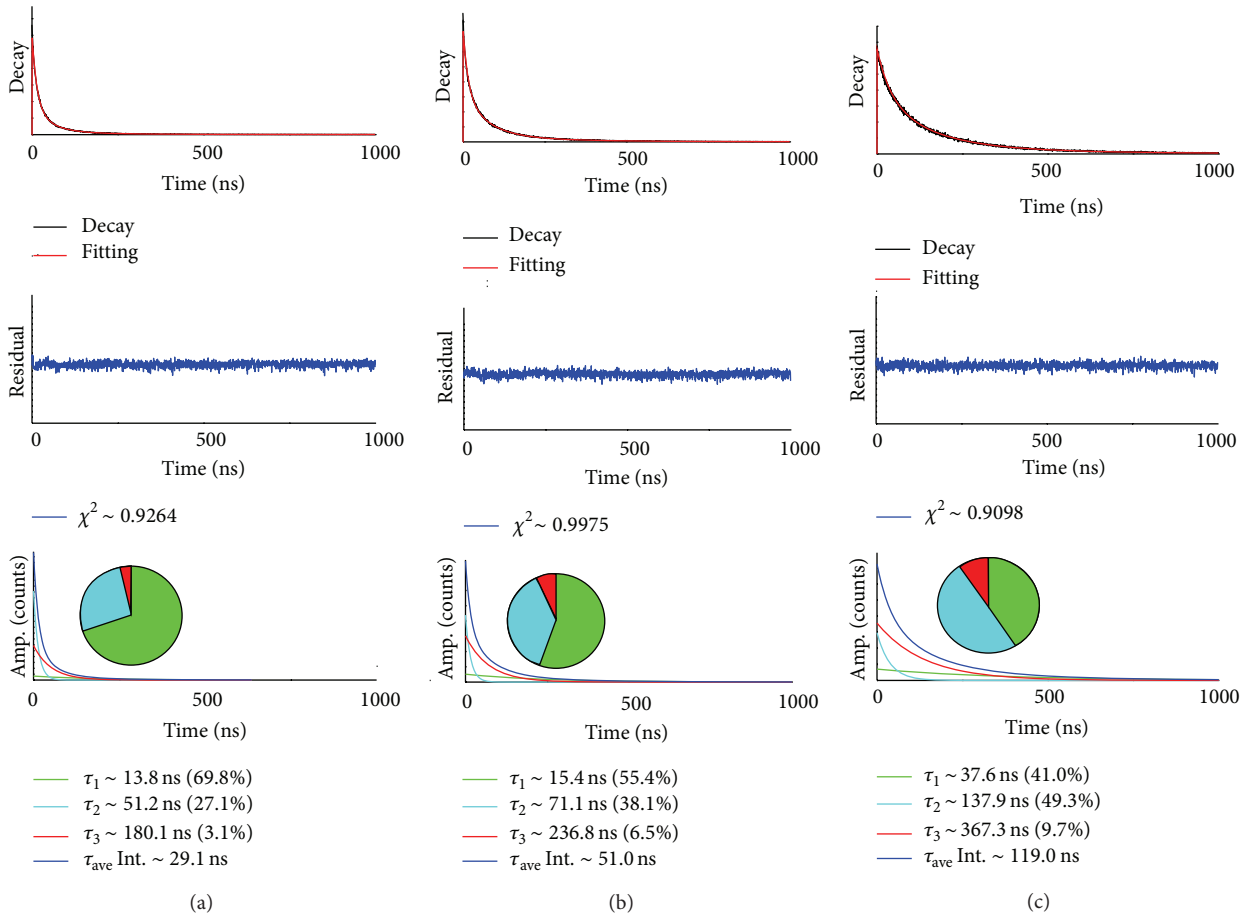

FIGURE 2: Emission intensity decays, residual traces, and exponential decay components of fractional emission amplitudes of CIS/$ZnS_{665\,nm}$ at (a) ~575 nm, (b) ~640 nm, and (c) ~690 nm on the microcover glass.

of Figure 4 display the thermal quenching of PLs from CIS/$ZnS_{555\,nm}$ and CIS/$ZnS_{665\,nm}$ which indicate the fast PL quenching due to thermalization above ~50 K. The PL of CIS/$ZnS_{555\,nm}$ has asymmetric spectral distribution, while the PL of CIS/$ZnS_{665\,nm}$ has a symmetric spectral distribution. It implies that the deep-trapped DA state is less size-dependent on the confinement compared to the shallow-trapped DA state and defect-related interface state. It is well known that the surface/interface defects of nanomaterials increase as the relative surface area per volume is increased by decreasing the size [23]. The temperature-resolved spectroscopy shows that the PL from the interface-trapped state and shallow-trapped DA state has less thermal quenching and the PL at longer wavelength from the deep-trapped DA state has stronger thermal quenching. The PL peak of CIS/$ZnS_{665\,nm}$ is shifted from ~670 nm to ~665 nm as the temperature is increased from 6 K to 300 K. The PL irradiance reduction of CIS/$ZnS_{555\,nm}$ at longer wavelength region is faster than that at shorter wavelength region as the temperature is increased. This implies the existence of stronger thermal ionization and phonon-assisted nonradiative decay at the deep-trapped DA state with the relatively stronger Coulomb interaction [24].

The FWHM (~115 nm) of PL spectrum from CIS/$ZnS_{665\,nm}$ is wider than that (~100 nm) of CIS/$ZnS_{555\,nm}$ at 300 K. However, the PL from CIS/$ZnS_{555\,nm}$ provides the better spectral coupling with the blue excitation for the hybrid white LEDs in the visible spectral region because CIS/$ZnS_{665\,nm}$ has the undesired infrared emission as shown in Figure 5(a). Figure 5(b) shows the proposed schematic sketch of CIS/ZnS coreshells stacking on the InGaN blue LEDs emitting at ~470 nm. The hybrid white LED is based on the integration of broad PL spectra from CIS/ZnS and blue emission from InGaN diodes. Figures 5(c), 5(d), and 5(e) display the photo pictures of devices and emissions of InGaN (c), hybrid white LED with CIS/$ZnS_{555\,nm}$ (d) and CIS/$ZnS_{665\,nm}$ (e), respectively.

4. Conclusion

CIS/$ZnS_{555\,nm}$ and CIS/$ZnS_{665\,nm}$ coreshells were utilized for developing the hybrid white LEDs where the nanoparticles were stacked on the blue LEDs. The time-resolved spectroscopy of CIS/$ZnS_{665\,nm}$ revealed that the fast, intermediate, and slow decays were correlated to the interface-trapped state and shallow- and deep-trapped states, although the three

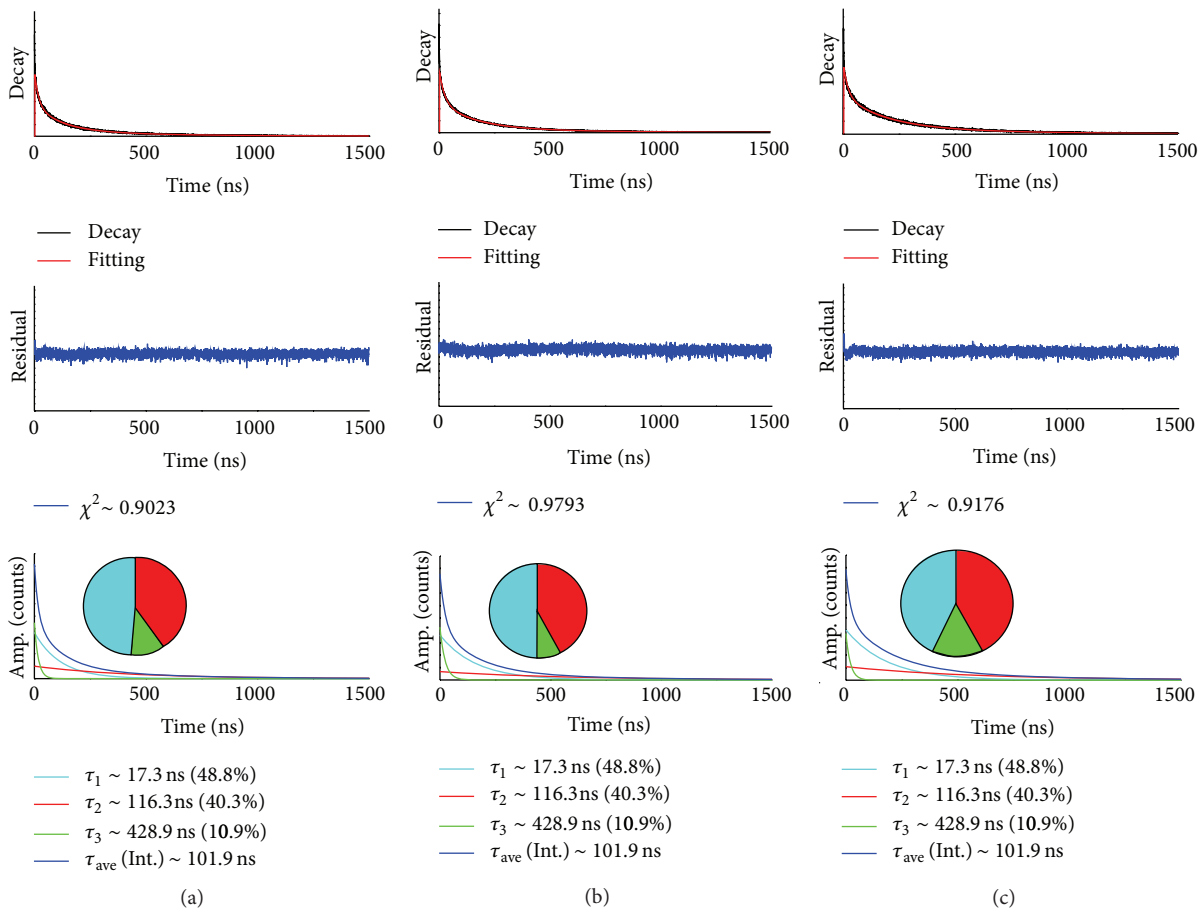

FIGURE 3: Emission intensity decays, residual traces, and exponential decay components of fractional emission amplitudes of CIS/$ZnS_{555\,nm}$ at (a) ~525 nm, (b) ~550 nm, and (c) ~600 nm on the microcover glass.

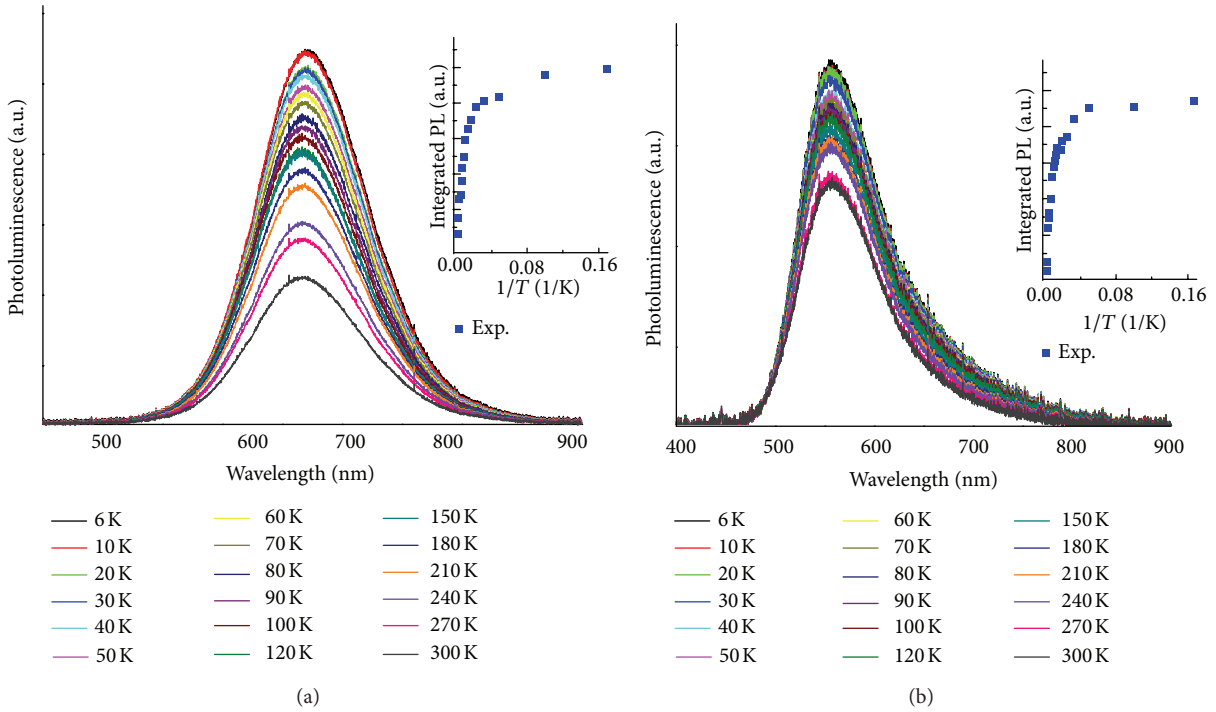

FIGURE 4: Photoluminescence spectra of (a) CIS/$ZnS_{665\,nm}$ and (b) CIS/$ZnS_{555\,nm}$ and quenching trend (inset).

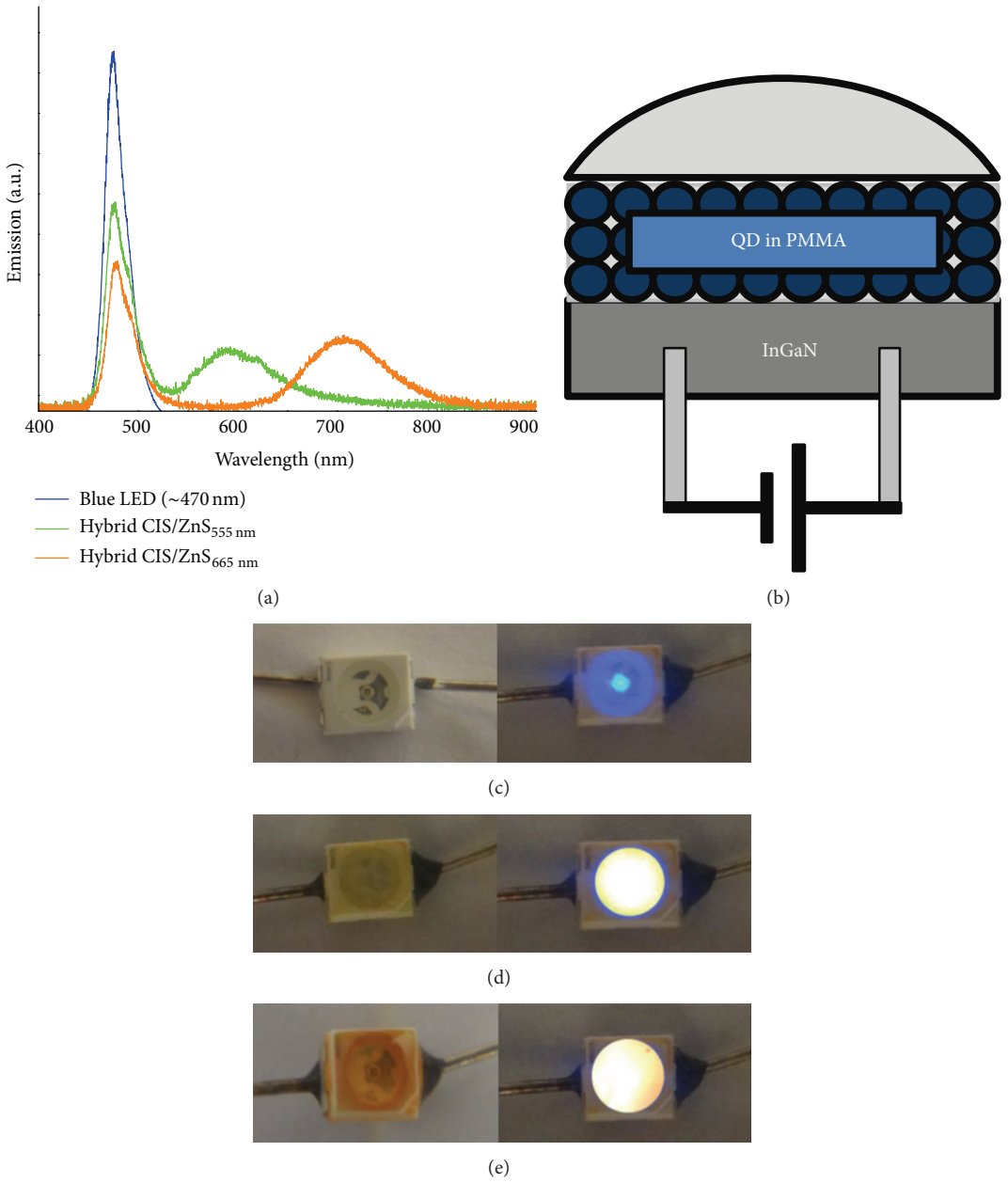

Figure 5: (a) Emission spectra of InGaN, hybrid LED with CIS/$ZnS_{555\,nm}$ and CIS/$ZnS_{665\,nm}$. (b) Proposed schematic sketch of CIS/ZnS stacking on the InGaN LED. Photo pictures of devices and emissions of (c) InGaN, (d) hybrid white LED with CIS/$ZnS_{555\,nm}$, and (e) hybrid white LED with CIS/$ZnS_{665\,nm}$.

exponential decays are distributed in the entire spectra. The asymmetry of PL spectrum and the reduced spectral width of the CIS/$ZnS_{555\,nm}$ imply that the deep-trapped DA state is less size-dependent on the quantum confinement compared to the shallow-trapped DA state and defect-related interface state. The temperature-resolved spectroscopy revealed that the PL from deep-trapped DA state has a relatively large thermal quenching through the thermal ionization and the phonon-assisted nonradiative decay due to the stronger Coulomb interaction of deep-trapped DA pairs, while the PLs from interface defect state and shallow-trapped DA state have relatively less thermal quenching due to the weak Coulomb interaction at the near outer boundary of the nanocrystal. The spectral coupling between the PL from CIS/ZnS with a broad spectral width and the blue diode excitation leads to the realization of hybrid white LEDs.

Conflict of Interests

The authors declare that there is no conflict of interests regarding the publication of this paper.

Acknowledgments

The work at HU was supported by the NSF HRD-1137747 and ARO W911NF-11-1-0177.

References

[1] J. Zhang, R. Xie, and W. Yang, "A simple route for highly luminescent quaternary Cu-Zn-In-S nanocrystal emitters," *Chemistry of Materials*, vol. 23, no. 14, pp. 3357–3361, 2011.

[2] W.-S. Song and H. Yang, "Fabrication of white light-emitting diodes based on solvothermally synthesized copper indium sulfide quantum dots as color converters," *Applied Physics Letters*, vol. 100, no. 18, Article ID 183104, 4 pages, 2012.

[3] Y. Zhang, C. Xie, H. Su et al., "Employing heavy metal-free colloidal quantum dots in solution-processed white light-emitting diodes," *Nano Letters*, vol. 11, no. 2, pp. 329–332, 2011.

[4] M. Uehara, K. Watanabe, Y. Tajiri, H. Nakamura, and H. Maeda, "Synthesis of CuInS2 fluorescent nanocrystals and enhancement of fluorescence by controlling crystal defect," *The Journal of Chemical Physics*, vol. 129, no. 13, Article ID 134709, 2008.

[5] Z. Peng and X. Peng, "Formation of high-quality CdTe, CdSe, and CdS nanocrystals using CdO as precursor," *Journal of the American Chemical Society*, vol. 123, no. 1, pp. 183–184, 2001.

[6] D. R. Baker and P. V. Kamat, "Tuning the emission of CdSe quantum dots by controlled trap enhancement," *Langmuir*, vol. 26, no. 13, pp. 11272–11276, 2010.

[7] H. Zhong, Y. Zhou, M. Ye et al., "Controlled synthesis and optical properties of colloidal ternary chalcogenide $CuInS_2$ nanocrystals," *Chemistry of Materials*, vol. 20, no. 20, pp. 6434–6443, 2008.

[8] Y. Hamanaka, T. Kuzuya, T. Sofue, T. Kino, K. Ito, and K. Sumiyama, "Defect-induced photoluminescence and third-order nonlinear optical response of chemically synthesized chalcopyrite $CuInS_2$ nanoparticles," *Chemical Physics Letters*, vol. 466, no. 4–6, pp. 176–180, 2008.

[9] W. Zhang, Q. Lou, W. Ji, J. Zhao, and X. Zhong, "Color-tunable highly bright photoluminescence of cadmium-free cu-doped Zn-In-S nanocrystals and electroluminescence," *Chemistry of Materials*, vol. 26, no. 2, pp. 1204–1212, 2014.

[10] S. L. Castro, S. G. Bailey, R. P. Raffaelle, K. K. Banger, and A. F. Hepp, "Synthesis and characterization of colloidal $CuInS_2$ nanoparticles from a molecular single-source precursor," *Journal of Physical Chemistry B*, vol. 108, no. 33, pp. 12429–12435, 2004.

[11] H. Y. Ueng and H. L. Hwang, "The defect structure of $CuInS_2$. part I: intrinsic defects," *Journal of Physics and Chemistry of Solids*, vol. 50, no. 12, pp. 1297–1305, 1989.

[12] V. K. Komarala, C. Xie, Y. Wang, J. Xu, and M. Xiao, "Time-resolved photoluminescence properties of CuInS 2/ZnS nanocrystals: Influence of intrinsic defects and external impurities," *Journal of Applied Physics*, vol. 111, no. 12, Article ID 124314, 2012.

[13] W. Zhang and X. Zhong, "Facile synthesis of ZnS-$CuInS_2$-alloyed nanocrystals for a color-tunable fluorchrome and photocatalyst," *Inorganic Chemistry*, vol. 50, no. 9, pp. 4065–4072, 2011.

[14] J. Seo, R. Fudala, W. J. Kim et al., "Hybrid optical materials of plasmon-coupled CdSe/ZnS coreshells for photonic applications," *Optical Materials Express*, vol. 2, no. 8, pp. 1026–1039, 2012.

[15] J. Seo, S. Raut, M. Abdel-Fattah et al., "Time-resolved and temperature-dependent photoluminescence of ternary and quaternary nanocrystals of $CuInS_2$ with ZnS capping and cation exchange," *Journal of Applied Physics*, vol. 114, no. 9, Article ID 094310, 2013.

[16] Y.-K. Kim, S.-H. Ahn, K. Chung, Y.-S. Cho, and C.-J. Choi, "The photoluminescence of $CuInS_2$ nanocrystals: effect of non-stoichiometry and surface modification," *Journal of Materials Chemistry*, vol. 22, no. 4, pp. 1516–1520, 2012.

[17] S. Neeleshwar, C. L. Chen, C. B. Tsai et al., "Size-dependent properties of CdSe quantum dots," *Physical Review B*, vol. 71, pp. 201307-1–201307-4, 2005.

[18] J. Wang, I. Mora-Seró, Z. Pan et al., "Core/shell colloidal quantum dot exciplex states for the development of highly efficient quantum-dot-sensitized solar cells," *Journal of the American Chemical Society*, vol. 135, no. 42, pp. 15913–15922, 2013.

[19] W. Chung, H. Jung, C. H. Lee, S. H. Park, J. Kim, and S. H. Kim, "Synthesis and application of non-toxic $ZnCuInS_2$/ZnS nanocrystals for white LED by hybridization with conjugated polymer," *Journal of the Electrochemical Society*, vol. 158, no. 12, pp. H1218–H1220, 2011.

[20] L. Li, T. J. Daou, I. Texier, T. T. K. Chi, N. Q. Liem, and P. Reiss, "Highly luminescent $CuInS_2$/ ZnS Core/Shell nanocrystals: cadmium-free quantum dots for in vivo imaging," *Chemistry of Materials*, vol. 21, no. 12, pp. 2422–2429, 2009.

[21] H. Kim, J. Y. Han, D. S. Kang et al., "Characteristics of CuInS2/ZnS quantum dots and its application on LED," *Journal of Crystal Growth*, vol. 326, no. 1, pp. 90–93, 2011.

[22] Q. Shen, I. Mora-Seró, Q. Shen et al., "High-efficiency "Green" quantum dot solar cells," *Journal of the American Chemical Society*, vol. 136, no. 25, pp. 9203–9210, 2014.

[23] P. Reiss, M. Protière, and L. Li, "Core/shell semiconductor nanocrystals," *Small*, vol. 5, no. 2, pp. 154–168, 2009.

[24] Y. K. Kim and C. J. Choi, "Tailoring the morphology and the optical properties of semiconductor nanocrystals by alloying," in *Nanocrystal*, Y. Masuda, Ed., chapter 14, 2011.

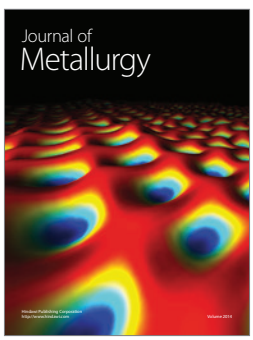

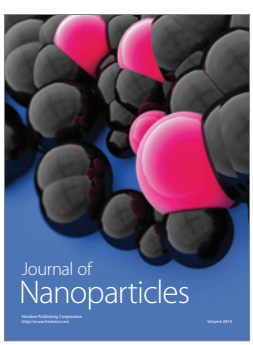

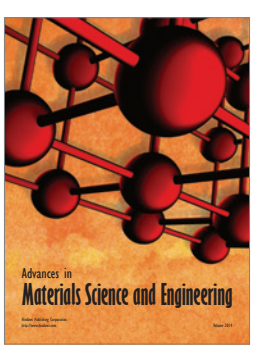

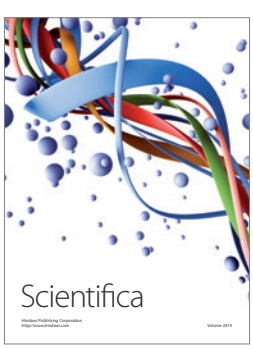

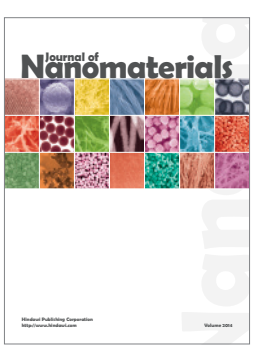

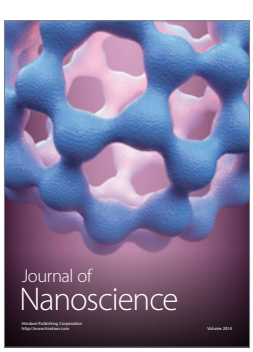

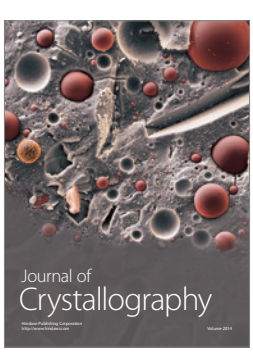

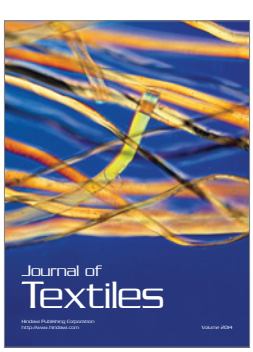

Hindawi

Submit your manuscripts at
http://www.hindawi.com